Astron. Astrophys. 296, 700–704 (1995)

ASTRONOMY AND ASTROPHYSICS

Multiple far-supercritical solutions for an $\alpha\Lambda$-dynamo

P. Muhli[1], **A. Brandenburg**[2], **D. Moss**[3], **and I. Tuominen**[1]

[1] Observatory, P.O. Box 14, FIN-00014 University of Helsinki, Finland
[2] HAO/NCAR*, P.O. Box 3000, Boulder, CO 80307, USA
[3] Mathematics Department, The University, Manchester M13 9PL, UK

Received 25 March 1994 / Accepted 17 September 1994

Abstract. We compute numerical solutions for axisymmetric, dynamically consistent mean-field dynamos in a spherical shell of conducting incompressible fluid. In the process of investigating the stability properties of solutions in the far-supercritical regime we found an unusual behaviour, with the magnetic energy decreasing discontinuously as the dynamo number is increased. A new stable solution with a more complicated field geometry emerges. In addition, a stable mixed parity state occurs at the discontinuity of the magnetic energy, between the two branches of stable pure parity solutions. For a given dynamo number there may be as many as four metastable solutions.

Key words: stars: magnetism – magnetic fields – MHD – dynamos

1. Introduction and basic equations

Stellar dynamos are often investigated using the mean-field approach, where the evolution of the mean magnetic field $\langle \boldsymbol{B} \rangle$ is described by

$$\frac{\partial \langle \boldsymbol{B} \rangle}{\partial t} = \mathrm{curl}(\langle \boldsymbol{u} \rangle \times \langle \boldsymbol{B} \rangle + \alpha \langle \boldsymbol{B} \rangle - \eta_t \mathrm{curl} \langle \boldsymbol{B} \rangle) \tag{1}$$

(e.g. Krause & Rädler 1980), where $\mathrm{div}\langle \boldsymbol{B} \rangle = 0$, and η_t is the turbulent magnetic diffusivity. The α parameter can have a non-vanishing value in the presence of helicity, which can lead to the generation of large-scale magnetic fields. The strength of this α–effect is characterized by a dynamo number $C_\alpha = \tilde{\alpha} R / \eta_t$, where $\tilde{\alpha}$ is a constant. The helicity, necessary for an α-effect, arises from the joint effects of the radial inhomogeneity of the convection zone and the Coriolis force. The resulting α is antisymmetric about the equatorial plane, and a particularly simple and often studied expression is $\alpha = \tilde{\alpha} \cos\theta$, where θ is the colatitude. In the present study anisotropies of α and η_t have been neglected (but see Rüdiger & Elstner 1994).

The magnetic back-reaction on the mean flow $\langle \boldsymbol{u} \rangle$ from the Lorentz force influences the flow via the mean-field momentum equation

$$\rho \frac{\mathrm{D}\langle \boldsymbol{u} \rangle}{\mathrm{D}t} = -\nabla \mathscr{P} + \langle \boldsymbol{J} \rangle \times \langle \boldsymbol{B} \rangle - \mathrm{Div}(\rho \mathscr{Q} - \mathscr{B}), \tag{2}$$

where $\mathscr{P}$ denotes a reduced pressure including gravitational potential and turbulent magnetic pressure. In Eq. (2), $\mathscr{Q}_{ij} = \langle u_i' u_j' \rangle$ and $\mathscr{B}_{ij} = \langle B_i' B_j' \rangle$ are, respectively, the Reynolds and Maxwell stress tensors, (e.g. Rüdiger et al. 1986; Rüdiger & Kitchatinov 1990). Eq. (2) is written in an inertial reference frame, and so the (conserved) angular momentum is specified by the initial condition on $\langle u_\phi \rangle$, and the Coriolis and centrifugal terms are automatically included.

In the presence of an anisotropy of the turbulent motions, correlations of different velocity components can drive a differential rotation via the so called Λ–effect, which parameterizes non-diffusive contributions to the (r, ϕ) and (θ, ϕ) components of $\mathscr{Q}$. For sufficiently slow rotation, the most important component is

$$\mathscr{Q}_{r\phi} = \Lambda_V \sin\theta \Omega - \nu_t r \sin\theta \partial\Omega/\partial r \tag{3}$$

(Rüdiger 1980), where $\Omega = \langle u_\phi \rangle / r \sin\theta$ and ν_t is a turbulent kinematic viscosity, for which we assume $\nu_t = \eta_t$, i.e. a turbulent magnetic Prandtl number of unity.

In this model, differential rotation is a self-consistent solution of the momentum equation, Eq. (2). When the dynamo equation, Eq. (1) and the momentum equation with non-zero Λ–effect are solved simultaneously, we are dealing with a dynamically consistent dynamo, sometimes referred to as an $\alpha\Lambda$–dynamo (Brandenburg et al. 1991, 1992). Malkus & Proctor (1975) and Proctor (1977) investigated dynamically consistent dynamos, where the macro-feedback (momentum equation) has been taken into account, and saturation was achieved by the so-called Malkus–Proctor mechanism. In their model there was no Λ–effect and differential rotation was therefore only driven by the large-scale magnetic field.

Send offprint requests to: P. Muhli

* The National Center for Atmospheric Research is sponsored by the National Science Foundation

The work of Proctor (1977) was restricted to antisymmetric (dipole-type) magnetic field configurations. Both antisymmetric and symmetric (quadrupole-type) solutions exist as a consequence of the perfect symmetries of the α and ω–effects. Either one or both of these solutions may be stable to axisymmetric perturbations, but more general calculations show that stable mixed parity solutions are also possible (Brandenburg et al. 1989), described by the parity parameter

$$P = \frac{E^{(S)} - E^{(A)}}{E^{(S)} + E^{(A)}}, \tag{4}$$

where $E^{(S)}$ and $E^{(A)}$ denote the energies in the symmetric (even, quadrupolar) and antisymmetric (odd, dipolar) parts of the magnetic field. The pure parity solutions with completely antisymmetric and symmetric fields are usually denoted by A0 and S0, respectively. Stable mixed parity solutions occur especially as the dynamo number, C_α, is increased. However, most of the known examples of mixed parity solutions are time dependent.

Usually the magnetic energy increases with increasing C_α. There are, however, examples with α–quenching where the magnetic energy reaches a maximum after which it decreases slightly before it levels off at a constant value (Meinel & Brandenburg 1990). In dynamos controlled by the Malkus–Proctor mechanism, the energy usually increases with C_α, and the energy of the S0 solution grows faster than the energy of the A0 solution, so there is a crossover at some value of C_α (Brandenburg et al. 1989). The stability problem of Malkus-Proctor solutions has recently excited some interest, because it appears that many axisymmetric solutions with weak differential rotation are unstable to nonaxisymmetric perturbations (Barker 1993; Barker & Moss 1993, 1994).

The purpose of this paper is to investigate the stability properties of solutions of an axisymmetric $\alpha\Lambda$–dynamo in the far-supercritical regime of C_α. During our investigation, we found a somewhat unusual behaviour, in that at a certain value of C_α the magnetic energy decreased abruptly and discontinuously. In the following we show that this behaviour is related to the emergence of a new solution with a lower magnetic energy and a more complicated field geometry at a particular value of C_α.

2. The model

We adopt the model of Brandenburg et al. (1991) for a dynamo consisting of an incompressible and electrically conducting fluid with constant and uniform density, ρ, in a rotating shell (cf. the sub-surface convective zone of a late type star) with inner and outer radii R_0 and R, respectively. This model is similar to that described in Brandenburg et al. (1992), except that the fluid is here assumed to be incompressible and thermodynamics are not included. We solve the hydromagnetic equations (see previous section) numerically in an inertial frame of reference for two quadrants (hemispheres) in order to examine the symmetry properties of the magnetic field and large-scale flow. For boundary conditions, we assume a perfect conductor without magnetic field below the convective shell ($r < R_0$), and a vacuum (current-free fields) outside the shell ($r > R$).

As initial condition we assume a rigid rotation with angular velocity Ω_0, and a weak "seed" magnetic field. The value of Ω_0 is prescribed in terms of the Taylor number, $\mathrm{Ta} = (2\Omega_0 R^2/\nu_t)^2$ and we use $\mathrm{Ta} = 10^6$. For R_0 and R, respectively, we use the values 0.7 and 1, expressed in units of the radius of the sphere. The initial parity, P_0 (cf. Eq. (4)), characterizes the symmetry of the initial magnetic field. In most of the cases we prescribed an initial value for P between +1 and −1 and allowed the parity subsequently to evolve with time.

We assume that α takes the form $\alpha = \tilde{\alpha}\cos\theta$, where the constant $\tilde{\alpha}$ is determined by the dynamo number C_α. Thus, α–quenching is neglected. We also neglect the Maxwell stress tensor $\mathscr{B}$, see Eq. (2), because its functional dependence on the mean fields is not well understood. The strength of the Λ–effect is described by $\Lambda_V = \nu_t V^{(0)}$, where we take $V^{(0)} = -1$. The sign of the parameter $V^{(0)}$ determines the sign of $\partial\Omega/\partial r$, strictly in the absence of magnetic field but, in practice, also with field present. Λ–quenching, i.e. magnetic back-reaction on the Λ-parameter, is neglected (but see Kitchatinov 1988).

In the following, length, time and the magnetic field are expressed in dimensionless form, i.e. length in units of R, time in units of the magnetic diffusion time, R^2/η_t, and $\langle \boldsymbol{B} \rangle$ in units of $(\mu_0\rho)^{1/2}\eta_t/R$, where μ_0 is the magnetic permeability. Typically the timestep, $\delta\tau$, we used in the runs was between 10^{-5} and 10^{-4}. Too long timesteps lead to numerical instabilities, whereas too small values are computationally prohibitive.

Most of the results presented here are for a resolution of 41×81 mesh points. Initially we performed computations on a mesh with 21×41 points and found qualitatively similar results. The energies changed by less than 10% and the values of C_α at which bifurcations occur changed by less than 5%, as the resolution was changed from 21×41 to 41×81. We expect that as we increased the resolution further any change would be rather smaller than this. Thus, we feel that the results presented below are qualitatively correct, but the numbers would change slightly if we used an even higher resolution.

We restrict ourselves to axisymmetric solutions. Although we have not checked whether the solutions are stable to non-axisymmetric perturbations, we anticipate that the differential rotation produced by the Λ-effect is large enough to cause non-axisymmetric structures to be wound-up rapidly, so leading to their enhanced dissipation (cf. Rädler 1986).

3. Results

In Fig. 1 we show the bifurcation diagram. Note the discontinuity at far-supercritical values of C_α, with stable mixed parity states for intermediate values of C_α. At the discontinuities the solution branches are expected to show infinite derivatives and continue as unstable solutions (e.g. Jennings & Weiss 1991). Using our time stepping method, such unstable solutions cannot be computed. Other methods could be used, such as those employed by Jennings (1991) for a simplified one-dimensional dynamo model. However, such methods are rather difficult to implement in more complicated multidimensional systems. Thus

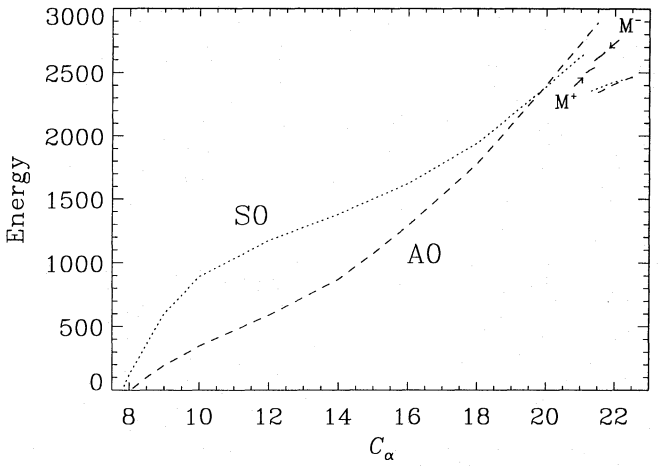

Fig. 1. Bifurcation diagram for the $\alpha\Lambda$-dynamo model with Ta = 10^6 and $V^{(0)} = -1$. All solutions depicted are stable and non-oscillatory. The dotted line connects S0-type solutions and the dashed line A0-type solutions. Note the discontinuity and the stable mixed parity states M^+ and M^-

we felt that a major effort to investigate such unstable solutions, which cannot physically be realized, was not justified at present.

At a particular value of C_α the type of the solution (S0, A0 or mixed parity state) depends only on the initial field parity, P_0. Below the far-supercritical regime, values of P_0 between –0.9 and –1 lead typically to the A0 case, whereas higher values of P_0 result in the S0 configuration.

The bifurcations of the S0 and A0 solutions from the trivial solution appear at $C_\alpha = 7.85$ and $C_\alpha = 8.1$, respectively. For smaller values of C_α all solutions are decaying. The energy in the bifurcation diagram is the total energy (nondimensional) of the mean magnetic field inside the "convection zone",

$$E = \frac{1}{2}\int_{CZ} \langle \boldsymbol{B} \rangle^2 dV. \quad (5)$$

At first, the energy of the S0 solution grows faster with C_α than the energy of the A0 solution. Beyond $C_\alpha \approx 14$ the energies of the A0 and S0 solutions begin to approach each other, and there is a crossover shortly before the discontinuity, at which the energy of the solutions abruptly decreases.

In Fig. 2 we present the magnetic fields and fluid velocities for the A0 solution at different values of C_α below the discontinuity. The geometry of the toroidal field becomes more complicated with increasing C_α, but still there is just one toroidal field belt in each hemisphere. The contours of constant angular velocity are almost perfectly cylindrical for small values of C_α, and the angular velocity increases towards the poles. Increasing C_α influences only slightly the angular velocity near the equatorial plane, but close to the poles Ω starts growing rapidly, reaching its maximum at the poles, at the bottom of the convective shell. The radial gradient of the angular velocity, $\partial\Omega/\partial r$, steepens with increasing C_α in the pole region.

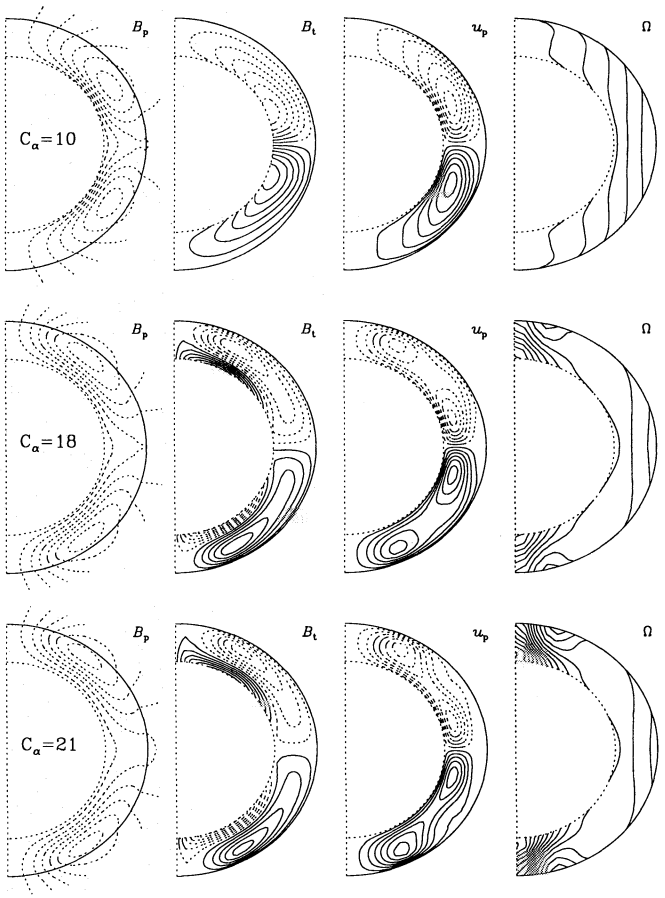

Fig. 2. Magnetic fields and fluid motions for stable, non-oscillatory A0 solutions with three different values of C_α . The columns show, from left to right, respectively the magnetic field lines of the poloidal field, contours of constant toroidal field, stream lines of the meridional motions and contours of constant angular velocity

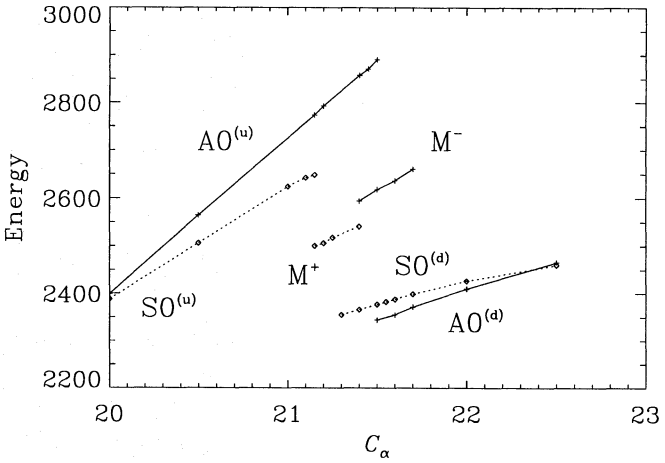

Fig. 3. The discontinuity between the upper (u) and lower (d) energy branches of the A0 and S0 solutions, obtained with a resolution of 41 × 81 mesh points

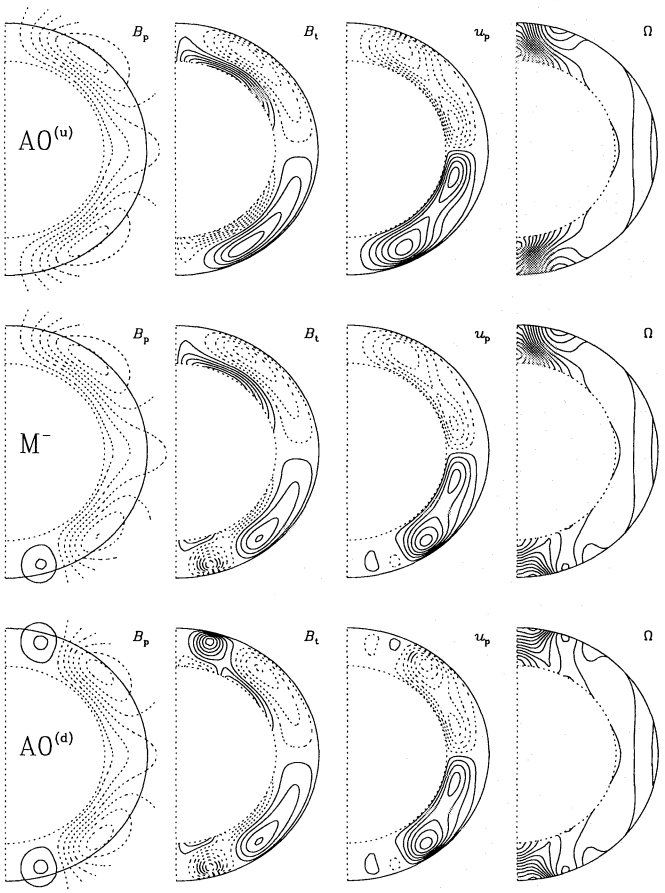

Fig. 4. Magnetic fields and fluid motions for the three different solutions of family A at $C_\alpha = 21.5$ (resolution 41 × 81 mesh points). From top to bottom respectively, the initial parities are −0.88, −0.85 and −0.80

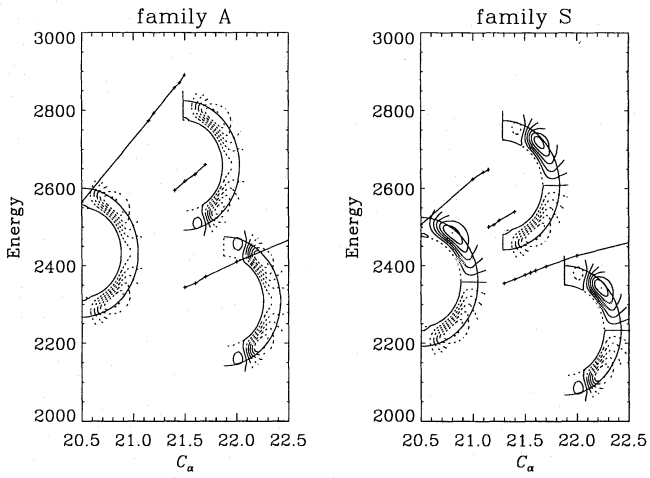

Fig. 5. The bifurcation diagram near the discontinuity presented separately for families A and S, with the corresponding poloidal fields (resolution 41 × 81 mesh points)

In Fig. 3 we show a "close-up" of the bifurcation diagram at the discontinuity. Clearly, there are two distinct families, which we call family A and family S. They both consist of two separate branches (upper and lower) divided by the energy "jump", and of a mixed parity state. The parity of the mixed parity state is $P \approx 0.61$ (M$^+$) in family S, and $P \approx -0.56$ (M$^-$) in family A. It is remarkable that the mixed parity state is indeed both steady and stable. In fact, all solutions presented here are steady if $C_\alpha \leq 22.5$. This is consistent with the differential rotation not being very strong (the conventional parameter $C_\Omega = \Delta\Omega R^2/\eta_t$ is only around 200). Also, the meridional flow is rather strong and delays the transition from steady to oscillatory solutions.

The field geometry changes at the discontinuity as abruptly as the energy of the mean magnetic field. This can be seen in Fig. 4, where we have plotted the magnetic fields and fluid velocities for the upper and lower branch solutions and for the mixed parity state of family A. In each case the value of C_α is the same, 21.5. Clearly, the lower branch solution, A0$^{(d)}$, shows two toroidal field belts in each hemisphere instead of just one. The mixed parity state represents an intermediate case with one toroidal field belt in one hemisphere. Where there are two toroidal field belts, the angular velocity is strongly decelerated at the pole, especially in the uppermost layer of the convective zone.

In Fig. 5 we have plotted the bifurcation diagram at the discontinuity separately for the A and S families and, for the purpose of better illustration, we also give the corresponding poloidal field geometries.

At some values of C_α there can be as many as four different types of (meta)stable solutions (Fig. 3). As we stated earlier, the initial parity, P_0, determines the type of the solution. We have presented this relation between P_0 and the type of the solution in Table 1 for three values of C_α. The table shows that one or two types of solutions appear only in a certain critical regime of P_0. For instance, at $C_\alpha = 21.4$ both mixed parity states were found in an extremely narrow range of P_0. At $C_\alpha = 21.5$ the lower branch A0 solution came up for just one value of P_0. Therefore it is possible that, by carrying out a large number of simulations with very small increments of P_0 around the critical regime, more than four different solutions could be found at some value of C_α. (But note that our initial field *geometry* is a 'hidden variable' – we fixed this arbitrarily and chose to vary P_0. With a different choice of the geometry, the relation between P_0 and the final state might be slightly different.)

Table 1. The relation between P_0 and the type of the solution for three values of C_α (resolution 41 × 81 mesh points)

$C_\alpha \rightarrow$	21.4	21.5	21.6
S0$^{(d)}$	≥ -0.79	≥ -0.79	≥ -0.79
M$^+$	−0.793	–	–
A0$^{(d)}$	–	−0.8	≤ -0.99
M$^-$	−0.8.. − 0.795	−0.86.. − 0.82	−0.95.. − 0.8
A0$^{(u)}$	≤ -0.81	≤ -0.865	–
S0$^{(u)}$	–	–	–

Beyond $C_\alpha = 22.5$ we carried out only a few simulations and most of them with the lower resolution. At $C_\alpha = 23.2$ we found "semi-oscillating" A0 and S0 solutions which show irregular, chaotic "pulses" of the otherwise steady magnetic energy and parity, with a duration of ≈ 0.2. The "pulses" emerged with a period of ≈ 0.5 and ≈ 0.8 for the S0 and A0 cases, respectively, though the period seemed to become gradually longer with time. Above $C_\alpha = 23.5$ we found steadily oscillating solutions. Their energy amplitude and cycle period decreases with increasing C_α. The largest value of C_α we used in the simulations was 25.

4. Astrophysical implications

Our results might have important astrophysical implications for stars where the dominant feedback on the dynamo is from the large scale fluid motions driven by the Lorentz force of the mean magnetic field. The dependence on the dynamo number C_α may be understood as a dependence on the angular velocity of the star. Of course, Ta is also a function of the angular velocity, and we have kept this constant, so our remarks cannot be more than speculative and incomplete. The dependence of the magnetic energy on C_α would then possibly correspond to a dependence of measures of stellar activity (e.g. the Ca II HK emission) on stellar rotation rate. Based on our results, we might expect under certain conditions a sudden drop in the stellar activity parameter above some critical rotation speed.

Such a behaviour has not been observed so far. However, it may be useful to recall a related behaviour where the (appropriately normalized) stellar cycle frequency is observed to increase with the inverse Rossby number along two disconnected branches (Saar & Baliunas 1992). Our model is too simple and cannot be applied to such particular cases, especially because in the parameter regime displayed here all solutions are non-oscillatory. Nevertheless, we suspect that the discontinuous behaviour observed for stellar cycle frequencies might be a consequence of a systematic change in the field geometry of the type similar to that seen in the present paper.

Most of our knowledge concerning the dependence of stellar activity parameters on the angular velocity is currently based on the Mt. Wilson Ca II time series. However, in the near future extensive results for giant stars in clusters are to be expected (Baliunas et al., private communication). This is interesting because it offers the possibility that new patterns of activity may appear.

References

Barker D. M., 1993, in: Theory of Solar and Planetary Dynamos, NATO ASI, eds. P.C. Matthews, A.M. Rucklidge, Cambridge University Press, p. 27
Barker D. M., Moss D., 1993, in: The Cosmic Dynamo, IAU Symposium No. 157, eds. F. Krause et al., Kluwer Acad. Publ., Dordrecht, p. 147
Barker D. M., Moss D., 1994, A&A 283, 1009
Brandenburg A., Krause F., Meinel R., Moss D., Tuominen I., 1989, A&A 213, 411
Brandenburg A., Moss D., Rüdiger G., Tuominen I., 1991, Geophys. Astrophys. Fluid Dyn. 61, 179
Brandenburg A., Moss D., Tuominen I., 1992, A&A 265, 328
Jennings R. L., 1991, Geophys. Astrophys. Fluid Dyn. 57, 147
Jennings R., Weiss N. O., 1991, MNRAS 252, 249
Kitchatinov L. L., 1988, Astron. Nachr. 309, 197
Krause F., Rädler K.-H., 1980, Mean-Field Magnetohydrodynamics and Dynamo Theory, Akademie-Verlag, Berlin
Malkus W. V. R., Proctor M. R. E., 1975, J. Fluid. Mech. 67, 417
Meinel R., Brandenburg A., 1990, A&A 238, 369
Proctor M. R. E., 1977, J. Fluid. Mech. 80, 769
Rädler K.-H., 1986, Plasma Physics, ESA SP-251, 569
Rüdiger G., 1980, Geophys. Astrophys. Fluid Dyn. 16, 239
Rüdiger G., Elstner D., 1994, A&A 281, 46
Rüdiger G., Kitchatinov L. L., 1990, A&A 236, 503
Rüdiger G., Tuominen I., Krause F., Virtanen H., 1986, A&A 166, 306
Saar S. H., Baliunas S. L., 1992, in: The Solar Cycle, ed. K.L. Harvey, ASP Conf. Series 27, p. 150

This article was processed by the author using Springer-Verlag LaTeX A&A style file version 3.